PAPER

Tunneling induced swapping of orbital angular momentum in a quantum dot molecule

IOP Publishing | Astro Ltd Laser Physics

Laser Phys. **33** (2023) 096001 (8pp) https://doi.org/10.1088/1555-6611/ace250

Tunneling induced swapping of orbital angular momentum in a quantum dot molecule

S I S Al-Hawary[1,*], Wesam R Kadhum[2,13], E Abdu Musad Saleh[3], Y Yacin[4], E Adnan Abdullah[5], M T Qasim[6], B Abdullaeva[7], I B Sapaev[8,9], M Abdulfadhil Gatea[10,11] and A Alsalamy[12]

[1] Department of Business Administration, Business School, Al al-Bayt University, P O BOX 130040, Mafraq 25113, Jordan
[2] Department of Pharmacy, Kut University College, Kut 52001, Wasit, Iraq
[3] Department of Chemistry, Prince Sattam Bin Abdulaziz University, College of Arts and Science, Wadi Al-Dawasir 11991, Saudi Arabia
[4] Medical Technical College, Al-Farahidi University, Baghdad, Iraq
[5] Department of Radiology and Sonar Technologies, Al Rafidain University College, Bagdad, Iraq
[6] Department of Anesthesia, College of Health and Medical Technology, Al-Ayen University, Thi-Qar, Iraq
[7] Vice-Rector for Scientific Affairs, Tashkent State Pedagogical University, Tashkent, Uzbekistan
[8] Tashkent Institute of Irrigation and Agricultural Mechanization Engineers, National Research University, Tashkent, Uzbekistan
[9] New Uzbekistan University, Tashkent, Uzbekistan
[10] Technical Engineering Department College of Technical Engineering, The Islamic University, Najaf, Iraq
[11] Department of Physics, College of Science, University of Kufa, Kufa, Iraq
[12] College of Medical technique, Imam Ja'afar Al-Sadiq University, Al-Muthanna 66002, Iraq
[13] Advanced research center, Kut university college, Kut 52001, Waist, Iraq

E-mail: dr_sliman73@aabu.edu.jo

Received 1 June 2023
Accepted for publication 21 June 2023
Published 11 July 2023

Abstract

In this paper, we have examined the effectiveness exchange of optical vorticity via three-wave mixing (TWM) technique in a four-level quantum dot (QD) molecule by means of the electron tunneling effect. Our analytical analysis demonstrates that the TWM procedure can result in the production of a new weak signal beam that may be absorbed or amplified within the QD molecule. We have taken into account the electron tunneling as well as the relative phase of the applied lights to assess the absorption and dispersion characteristics of the newly generated light. We have discovered that the slow light propagation and signal amplification can be achieved. Our results show that the exchange of the orbital angular momentum of light can transfer from coupling optical vortex light to the new generated light in high efficiency.

Keywords: three-wave mixing, tunneling, quantum dot, orbital angular momentum

(Some figures may appear in colour only in the online journal)

* Author to whom any correspondence should be addressed.

1. Introduction

Multi-wave mixing, which relies on quantum coherence and quantum interference, constitutes a nonlinear optical process of utmost importance and interest. A plethora of researchers have delved into its theoretical and experimental aspects in recent years, given its vast potential for applications in nonlinear optics, including but not limited to electromagnetically induced transparency (EIT) [1], electromagnetically induced grating [2, 3], optical bistability [4, 5], enhanced Kerr nonlinearity [6] and others [7–9]. It is widely acknowledged that the strength of the generated field signal in multi-wave mixing is directly proportional to its conversion efficiency. As such, researchers have devoted significant resources to enhancing the conversion efficiency of multi-wave mixing through various approaches. In light of this, the conversion efficiency of multi-wave mixing has been scrutinized utilizing the EIT mechanism in multi-level atomic systems [7, 10, 11]. For example, Wu *et al* investigated four-wave mixing (FWM) scheme in a five-level atomic system based on EIT [7]. The phenomenon of EIT has been extensively investigated, revealing its ability to effectively inhibit both two-photon and three-photon absorptions in the FWM scheme. This enables FWM to proceed through real, resonant intermediate states without any discernible loss due to absorption. In another study by Zubairy group [10], a discussion regarding an effective frequency conversion strategy using Autler-Townes splitting (ATS) in lieu of the widely recognized EIT mechanism in a three-level quantum system has been presented. It has been discovered that the targeted system can be utilized to execute the customary three-level EIT phenomenon. Furthermore, a concrete documentation has been suggested as proof of the collapse of nonlinear processes facilitated by EIT. This proposition provides a compelling indication that prior physical intuition regarding the implementation of the standard EIT technique in nonlinear optics may not be adequately comprehensive. Recent findings reveal that the transference of orbital angular momentum (OAM) of light can be transferred from optical vortex lights to a newly generated light through the utilization of the FWM mechanism [12–14]. For example, Asadpour *et al* studied the exchange of OAM stated of light in a symmetric broken quantum system in ATS and EIT regimes [13]. In recent years, with the emergence of new materials, i.e. quantum wells (QWs) and quantum dots (QDs) [15–18], researchers have paid much attention to the FWM process in these materials because of their excellent properties [19, 20]. These structures have large electric dipole moments, small effective electric mass, and highly nonlinear optical coefficients in comparison to atomic systems [21–23]. Moreover, the dipole moments, intersubband energies, and electron function symmetries can be meticulously tailored by carefully selecting the constituent materials and structural dimensions. In the existing literature, there exists a plethora of investigations that document the quantum coherence and interference phenomena in semiconductor QWs and QDs structures [24–32]. The current study focuses on the interaction between laser beams and QDs. It has been demonstrated that the existence of inter-dot tunneling leads to the generation of an additional laser beam when a single probe beam is initially directed towards one transition of the four-level QDs. Analytical solutions have been presented to elucidate this particular scenario. Furthermore, it has been revealed that the high conversion efficiency for the two-wave mixing (TWM) mechanism can be attributed to the impact of inter-dot tunneling, which can be regulated by an external electric voltage. At the end it has been shown that when the strong coupling light becomes optical vortex light, the winding number can be transferred to the new generated light with high exchange efficiency.

2. Model and formulation

A four-level quantum dot molecule (QDM) with electron tunneling effect is shown in figure 1. A weak probe field with Rabi frequency Ω_p and detuning δ acts on transition $|1\rangle \leftrightarrow |2\rangle$. The transition $|3\rangle \leftrightarrow |4\rangle$ is coupled by a strong coupling field by Rabi frequency Ω_c. The levels $|2\rangle$ and $|3\rangle$ are derived by electron tunneling processes T_e. The interaction Hamiltonian of the system after the dipole and rotating-wave approximations is given as follow:

$$\begin{aligned} H = &\sum_j \varepsilon_j |j\rangle\langle j| + T_e |2\rangle\langle 3| \\ &- \hbar[\Omega_p^* e^{i\delta t} |1\rangle\langle 2| + \Omega_p^* e^{-i\delta_c t} |4\rangle\langle 3| \\ &+ \Omega_s^* e^{i\delta_s t} |1\rangle\langle 4| + H.c] \end{aligned} \tag{1}$$

where ε_j is the energy of the states $|j\rangle$ and δ_i corresponds to the frequency detuning of the applied lights. The time-dependent probability amplitude for discovering particles in the appropriate subbands is denoted by $A_j\,(j = 1-4)$ and it is assumed that the state wave function has the form $|\Psi(t)\rangle = A_1(t)|1\rangle + A_2(t)|2\rangle + A_3(t)|3\rangle + A_4(t)|4\rangle$. When $|\Psi\rangle$ is added to the Schrodinger equation $i\partial\Psi/\partial t = H_{\text{int}}^I \Psi$, the probability amplitudes equation is obtained:

$$\frac{\partial A_1}{\partial t} = i\Omega_p^* A_2 + i\Omega_s^* A_4 \tag{2}$$

$$\frac{\partial A_2}{\partial t} = i(-\delta + i\Gamma_2)A_2 + i\Omega_p A_1 + iT_e A_3 \tag{3}$$

$$\frac{\partial A_3}{\partial t} = i(-\omega_{32} + i\Gamma_3)A_3 + iT_e A_2 + i\Omega_c^* A_4 \tag{4}$$

$$\frac{\partial A_4}{\partial t} = i(-\Delta_c + i\Gamma_4)A_4 + i\Omega_s A_1 + i\Omega_c A_3. \tag{5}$$

In the above equations, we set $\Gamma_2 = \Gamma_3 = \Gamma_4 = \gamma$ and $\omega_{32} = 0$. In this present study, our objective is to determine the amplitude of the light generated through the utilization of the esteemed Maxwell equations. The Maxwell equations, in the context of the slowly varying envelope approximation and under the assumption of time-independent probe light, provide the necessary framework for understanding the behavior of two weak probe and signal light waves that propagate along the z-axis

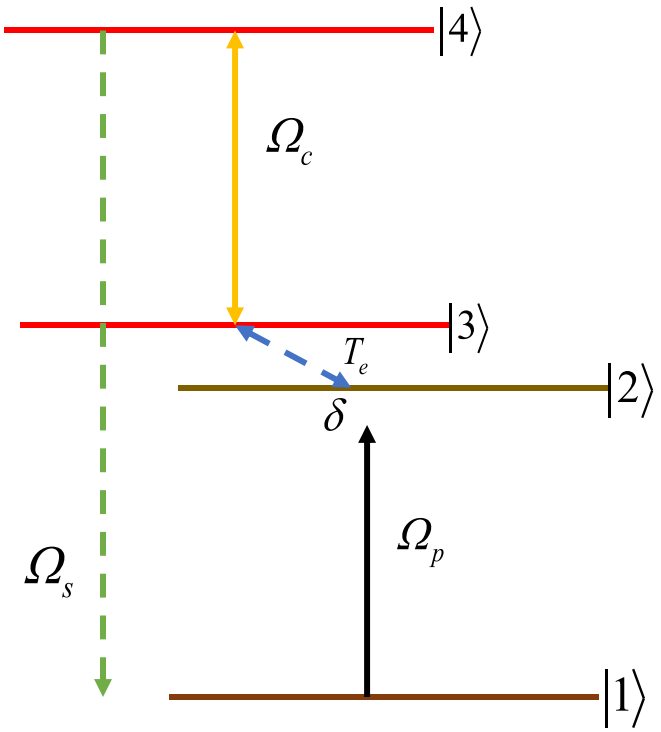

Figure 1. The four-level quantum dot molecule in the presence of the electron tunneling T_e which interacts by a weak probe light, a coupling light and a new generated signal light.

$$\frac{\partial \Omega_p}{\partial z}+\frac{1}{c}\frac{\partial \Omega_p}{\partial t}=\frac{1}{2k_p}\nabla_{\perp}^2\Omega_p+ik_pA_2A_1^*, \tag{6}$$

$$\frac{\partial \Omega_s}{\partial z}+\frac{1}{c}\frac{\partial \Omega_s}{\partial t}=\frac{1}{2k_s}\nabla_{\perp}^2\Omega_s+ik_sA_4A_1^*, \tag{7}$$

$k_{p(s)}$ is the wave number of the probe field (the TWM field). The first terms on the right-hand side of equations (6) and (7) stand for the transverse variations of the probe and TWM fields, which are responsible for the diffraction either in the medium or in vacuum, which can be neglected if the propagation distance z is much smaller than the Rayleigh ranges of the probe field or the TWM field. The aforementioned probability amplitude equations, as stated in equations (2)–(5), necessitate simultaneous solution with Maxwell's equation, presented in equations (6) and (7), in a manner that is self-consistent. Prior to endeavoring to solve the nonlinear equations, it is prudent to initially examine the linear excitation of the system, as it proffers valuable insights for the weak nonlinear theory. We suppose that the Rabi frequencies of the probe pulse and TWM field,$\Omega_{p,s}$ are significantly lower than those of the CW pump field, Ω_c as a weak perturbation. One can execute the Fourier transformations for equations (2)–(5) when the electrons are initially occupied in the ground state, ($A_1 \simeq 1$), by specifying:

$$A_j=\frac{1}{\sqrt{2\pi}}\int_{-\infty}^{+\infty}A_j(\omega)\exp(-i\omega t)\mathrm{d}\omega, \qquad j=2,3,4 \tag{8}$$

$$\Omega_{p,s}(t)=\frac{1}{\sqrt{2\pi}}\int_{-\infty}^{+\infty}\Lambda_{p,s}(\omega)\exp(-i\omega t)\mathrm{d}\omega, \tag{9}$$

using the variable to represent the Fourier transform, equation (2) through (5) consequently assume the following form:

$$(\omega+i\gamma)a_3+T_ea_2+\Omega_c^*a_4=0, \tag{10}$$

$$(\omega-\delta+i\gamma)a_2+T_ea_3=-\Lambda_p, \tag{11}$$

$$(\omega-\Delta_d+i\gamma)a_4+\Omega_ca_3=-\Lambda_s, \tag{12}$$

$$\frac{\partial \Lambda_p}{\partial z}-i\frac{\omega}{c}\Lambda_p=ik_pa_2a_1^*, \tag{13}$$

$$\frac{\partial \Lambda_s}{\partial z}-i\frac{\omega}{c}\Lambda_s=ik_sa_4a_1^*, \tag{14}$$

where A_j and $\Lambda_{p,s}$ correspond to the Fourier transformations of A_j, and $\Omega_{p,s}$. Thus, we have:

$$a_2=-\frac{R_p(\omega)}{R(\omega)}\Lambda_p+\frac{R_1(\omega)}{R(\omega)}\Lambda_s, \tag{15}$$

$$a_4=\frac{R_s(\omega)}{R(\omega)}\Lambda_p+\frac{R_2(\omega)}{R(\omega)}\Lambda_s, \tag{16}$$

where

$$R_p(\omega)=-(\omega+i\gamma_3)(\omega-\Delta_c+i\gamma_4)+|\Omega_c|^2 \tag{17}$$

$$R_1(\omega)=-\Omega_c^*T_e, \tag{18}$$

$$R_s(\omega)=-\Omega_cT_e \tag{19}$$

$$R_2(\omega)=|\Omega_c|^2-(\omega+i\gamma_3)(\omega-\delta+i\gamma_2), \tag{20}$$

$$\begin{aligned}R(\omega)=&(\omega+i\gamma_3)(\omega-\delta+i\gamma_2)(\omega-\Delta_c+i\gamma_4)\\&-|T_e|^2(\omega-\Delta_d+i\gamma_4)-(\omega-\delta+i\gamma_2)|\Omega_c|^2.\end{aligned} \tag{21}$$

The analytical solutions for initial conditions for the probe pulse and TWM field, $\Lambda_p(0,\omega)$, and $\Lambda_s(0,\omega)=0$ can be given as follows:

$$\begin{aligned}\Lambda_p(z,\omega)=&\Lambda_p(0,\omega)[W_+(\omega)\exp(izK_+(\omega))\\&-W_-(\omega)\exp(izK_-(\omega))],\end{aligned} \tag{22}$$

$$\Lambda_s(z,\omega)=\Lambda_p(0,\omega)Q(\omega)[\exp(izK_-(\omega))-\exp(izK_+(\omega))]. \tag{23}$$

With

$$\begin{aligned}K_{\pm}(\omega)&=\frac{\omega}{c}-\frac{R_s(\omega)k_s+R_p(\omega)k_p\pm i\sqrt{G(\omega)}}{2R(\omega)}\\&=K_{\pm}(0)+K_{\pm}^1(\omega)+O(\omega^2)\end{aligned} \tag{24}$$

$$W_{\pm}(\omega) = \frac{R_p(\omega)k_p - R_s(\omega)k_s \pm \sqrt{G(\omega)}}{2\sqrt{G(\omega)}} = W_{\pm}(0) + O(\omega) \tag{25}$$

$$Q(\omega) = \frac{k_s R_s(\omega)}{\sqrt{Y(\omega)}} \tag{26}$$

$$G(\omega) = [R_p(\omega)k_p - R_s(\omega)k_s]^2 + 4R_1(\omega)R_2(\omega)k_p k_m. \tag{27}$$

The initial conditions for the pulsed probe and generated TWM fields at the entrance of the SQW structures at $z = 0$ are denoted by $\Lambda_{p,s}(0,\omega)$. It is important to note that there exist two modes, namely $K_{\pm}$ modes, which are described by the linearized dispersion relations $K = K_+(\omega)$ and $K = K_-(\omega)$, respectively. Typically, the dispersion relation can be expanded around the center frequencies of the probe pulse and TWM field, that is, $\omega = 0$ $\omega = 0$. Furthermore, it is customary to neglect higher-order terms, i.e.,$O(\omega^2)$ in $K_{\pm}(\omega)$ and $O(\omega)$ in $W(\omega)$. In general, the real part of $K_{\pm}(0)$ and the imaginary part of $K_{\pm}(0)$ represent the phase shifts and absorption coefficients per unit length, respectively. The group velocities $V_{g\pm}$ for $K_{\pm}$ modes are given by $1/\mathrm{Re}[K_{\pm}^{(1)}]$. Finally, applying an inverse Fourier transform to $\Lambda_{p,s}$ yields the desired result:

$$\Omega_{p,m}(z,t) = \frac{1}{\sqrt{2\pi}} \int_{-\infty}^{+\infty} \exp(-i\omega t)\Lambda_{p,s}(z,\omega)\mathrm{d}\omega \tag{28}$$

and henceforth, we shall present the linearized outcomes for both the probe pulse and the TWM field:

$$\Omega_p(z,t) = \Omega_p(0,\eta_+)A_+(0)e^{izK_+(0)} - \Omega_p(0,\eta_-)A_-(0)e^{izK_-(0)} \tag{29}$$

$$\Omega_s(z,t) = G(0)[\Omega_p(0,\eta_-)e^{izK_-(0)} - \Omega_p(0,\eta_+)e^{izK_+(0)}] \tag{30}$$

$\eta_{\pm} = t - z/V_{g\pm}$ and $\Omega_p(t) \equiv \Omega_p(z = 0,t)$ represent the initial probe pulse at $z = 0$. We use real-world parameters to showcase examples of enhancing TWM signals by tunneling effect based on the formulas shown in equations (29) and (30), which describe the propagation dynamics for the probe pulse and the generated TWM field. The K_+ mode decays significantly faster than the K_- mode, as evidenced by experiments. After a typical propagation distance, one may therefore safely ignore this quicker variable K_+. The probe and TWM pulses $\Omega_{p,s}$ can be rewritten as follows by ignoring the K_+ mode:

$$\Omega_p(z,t) = -\Omega_p(0,t - z/V_g)A_-(0)e^{iz\beta - z\alpha} \tag{31}$$

$$\Omega_S(z,t) = G(0)\Omega_p(0,t - z/V_g)e^{iz\beta - z\alpha} \tag{32}$$

where $V_g = 1/\mathrm{Re}[K_-^{(1)}]$ is the group velocity, $\alpha = \mathrm{Im}[K_-(0)]$ denotes the absorption coefficient, and $\beta = \mathrm{Re}[K_-(0)]$ represents the phase shift per unit length.

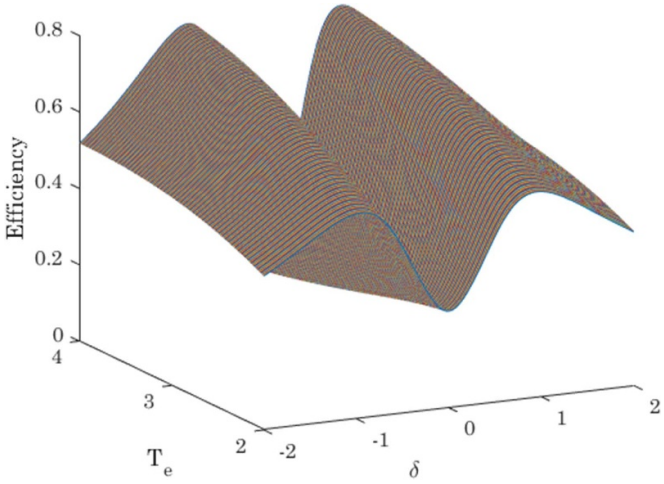

Figure 2. 3D plot of the efficiency versus probe detuning δ and electron tunneling T_e. The selected parameters are as $\alpha = 20$, $\Omega_c = \gamma, \phi = 0$ and Z = L.

3. Results

3.1. Three-wave mixing process

In this part, we investigate the effects of electron tunneling on the efficiency behavior of the TWM phenomenon. Here we show that due to the electron tunneling phenomenon, the efficiency of the TWM phenomenon improves and this can lead to many applications in quantum nonlinear optics. We next go on to the TWM field's conversion efficiency. The efficiency for the generated TWM field can be calculated as follows using the definition in [33]:

$$\rho = \left| E_s^{(\mathrm{out})}/E_p^{(\mathrm{in})} \right|^2, \tag{33}$$

where $E_s^{(\mathrm{out})}$ is the electric field $E_s(|E_s|^2 = 4\hbar^2|\Omega_s|^2/|\mu_{41}|^2)$ for the generated TWM field and $E_p(|E_p|^2 = 4\hbar^2|\Omega_p|^2/|\mu_{21}|^2)$ is the electric field for the probe pulse at the entrance $z = 0$. In figure 2, we show the efficiency curve in terms of detuning δ and tunneling parameter T_e. As can be seen, the efficiency value of the TWM phenomenon is completely dependent on the values of detuning parameters and tunneling intensity. We see that the efficiency value reaches 0.8 in the best parametric conditions. Therefore, it can be said that the proposed system has a suitable ability to improve the FWM phenomenon to a desired amount. In figure 3, we show the surface plot of the efficiency curve in terms of detuning and tunneling intensity. As can be seen, the value of TWM efficiency is high for high tunneling intensities T_e and non-zero detuning δ. This figure is in very good agreement with the results of figure 2.

In resonance condition of the probe light, i.e. $\delta = 0$, the efficiency as follows:

$$\rho = \left(\frac{E_m}{E_p}\right)^2 = \frac{|\mu_{21}|^2}{|\mu_{41}|^2} \frac{k_m^2(B)^2}{4k_m k_p(B)^2 + (C)^2} e^{-2\alpha Z}. \tag{34}$$

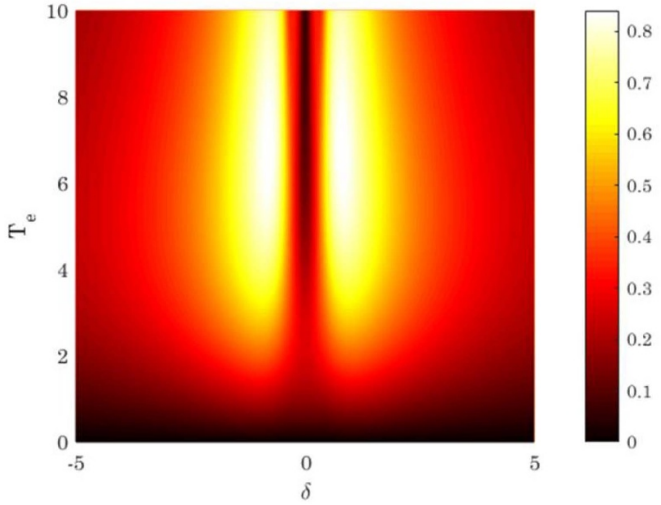

Figure 3. Surface plot of the efficiency versus probe detuning δ and electron tunneling T_e. The selected parameters are same as figure 2.

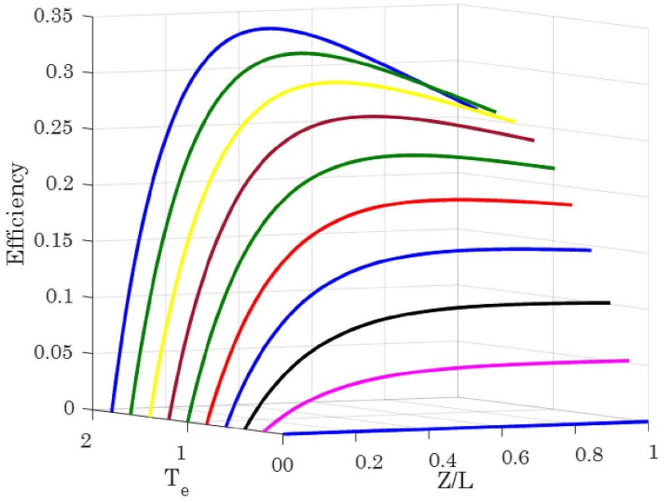

Figure 4. 3D plot of the efficiency versus propagation length Z/L and electron tunneling T_e. The selected parameters are same as figure 2.

With

$$C = k_m|T_e|^2 - k_p|\Omega_c|^2 + (k_s - k_p)\gamma^2 \tag{35}$$

$$B = \Omega_c T_e\,. \tag{36}$$

From equation (34), one can find that the efficiency of the TWM process is dependent to the tunneling parameter and coupling field. In figure 4, we show the efficiency spectrum in terms of propagation length *Z*/*L* and tunneling intensity T_e. Here, we assume that the probe field is in resonant mode. As can be seen, in the absence of tunneling, the TWM phenomenon does not occur. Therefore, the efficiency along the propagation path is zero. But with the increase of the tunneling amount, the efficiency value increases rapidly and then by propagation along the path, the efficiency value decreases and reaches a constant value. An important point is that for low tunneling intensities, the generated field during propagation is not absorbed along the path and the medium appears transparent to the generated light. But for higher intensities of tunneling T_e, some of the generated field is absorbed by the medium. Therefore, it can be said that the best mode for proper propagation of the generated light is low tunneling intensities. As we know, the absorption of the generated field is given by the imaginary term of the $K_-(0)$.

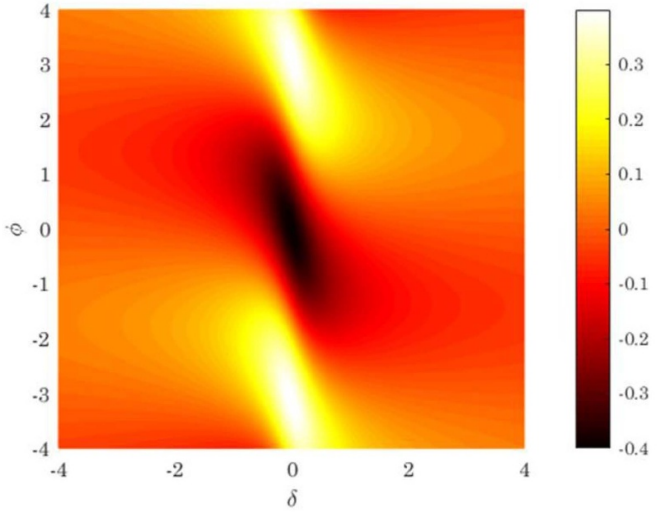

Figure 5. Surface plot of the new generated light absorption versus detuning δ and electron tunneling T_e. The selected parameters are same as figure 2.

Where parameter ϕ corresponds to the relative phase of applied lights. In figure 5, we show the absorption spectrum of the generated light in terms of probe detuning δ and relative phase $\phi = \phi_p + \phi_c - \phi_s$. It can be seen that the generated light in the areas related to $\delta = 0$, can have positive and negative value in different phases. As we know, the negative value in the absorption curve indicates the amplification in the system. Therefore, in the presence of the tunneling phenomenon in the QD, the generated field during the propagation is amplified. Of course, the amount of light absorption or amplification can be controlled by changing the relative phase of applied fields. Next and at the end, we will examine the group velocity of the generated light due to the TWM process. In figure 6, we show the group velocity of the new generated light versus probe detuning for different value of the relative phase. It can be seen that by adjusting the relative phase of the applied light the group velocity can be switched from slow to fast light or vice versa. Here, it can be seen that for relative phase $\phi = 0$ (solid line), the group velocity corresponds in the slow light level, however, for $\phi = \pi$ (dashed line) corresponds to the fast light. For relative phase $\phi = \pi/2$(dotted line), the group velocity is stopped in the medium. This result may have potential application in developing the quantum memory in quantum information technology.

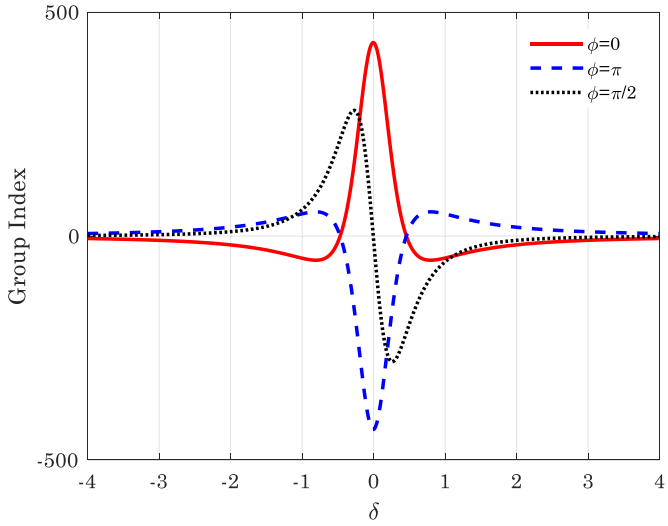

Figure 6. Group index of the new generated signal light versus probe detuning δ for different relative phase ϕ. The solid line corresponds to the $\phi = 0$, dashed line corresponds to the $\phi = \pi$ and dotted line corresponds to $\phi = \pi/2$. The selected parameters are same as figure 2.

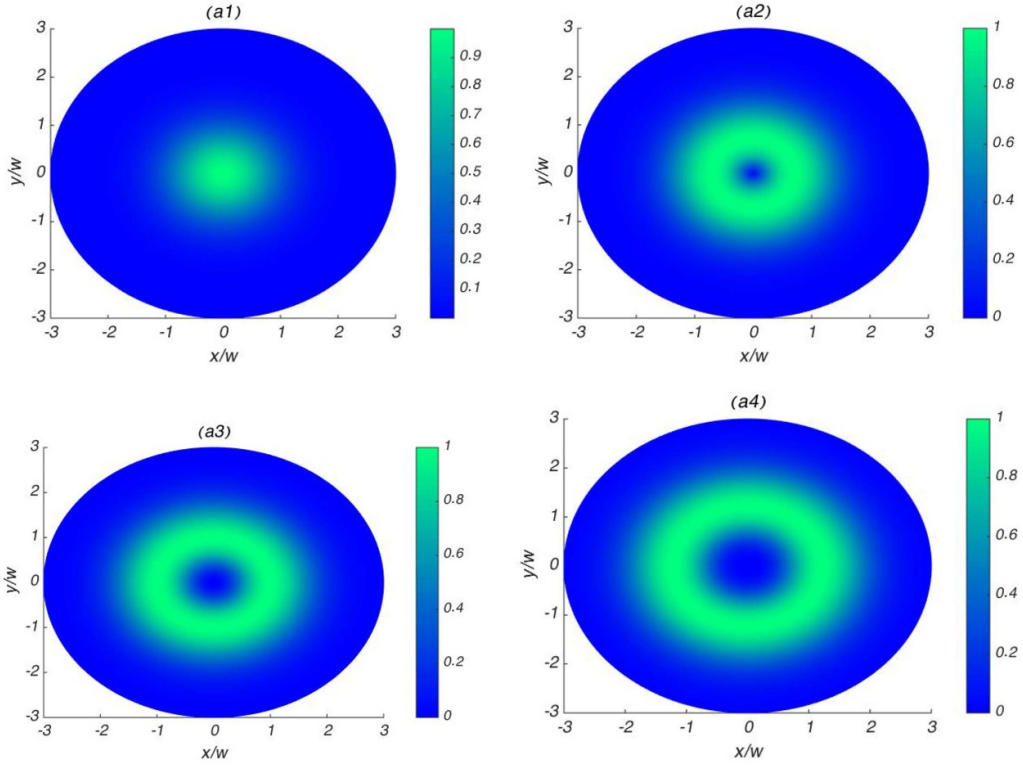

Figure 7. Intensity distribution for different OAM number of vortex light. (a_1) $l_c = 0$, (a_2) $l_c = 1$, (a_3) $l_c = 2$ and (a_4) $l_c = 3$. The selected parameters are same as figure 2.

3.2. *Exchange of OAM of light*

Let us now turn our attention to the spatial profile of the laser fields described by:

$$\Omega = \Omega_0 \frac{1}{\sqrt{|l|!}} \left(\frac{\sqrt{2}r}{w}\right)^{|l|} \times L_p^{|l|}\left(\frac{2r^2}{w^2}\right) e^{-r^2/w^2} e^{il\varphi} \tag{37}$$

where, Ω, w, l and p show the constant Rabi frequency, beam waist radius, azimuthal (OAM) and Radial indices of the LG mode, respectively. Here, the associated Laguerre polynomial $L_p^{|l|}(x)$ has the form:

$$L_p^{|l|}(x) = \frac{e^x x^{-|l|}}{p!} \frac{d^p}{dx^p} \left| x^{|l|+p} e^{-x} \right|. \tag{38}$$

With $x = 2r^2/w^2$ determining the radial dependence of the LG beams for different radial mode numbers. When l is not

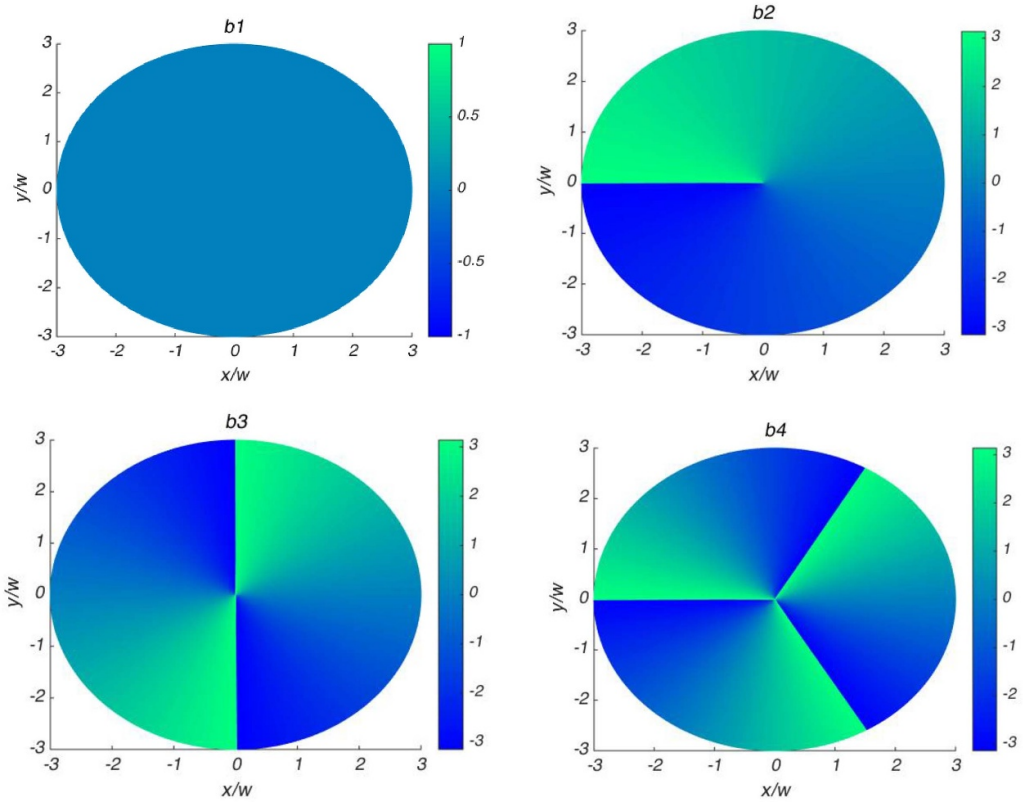

Figure 8. Phase distribution for different OAM number of vortex light. (b_1) $l_c = 0$, (b_2) $l_c = 1$, (b_3) $l_c = 2$ and (b_4) $l_c = 3$. The selected parameters are same as figure 2.

zero, the LG light beams possess OAM along the optical axis. The Rabi frequency of the third field generated is linked to both the inter-dot tunneling as well as the Rabi frequency of the probe and strong control fields. Henceforth, the generated laser field Ω_s takes on a vortex form if either or both of the fields Ω_p and Ω_c are initially in a vortex state. This transfer of optical vortices is attributed to the presence of interdot tunneling, which can be regulated by means of an external electric voltage. For the purposes of this discussion, we posit that the Ω_c is optical vortex light with zero radial index $p = 0$, and is given as follows:

$$\Omega_c = \varepsilon_c \frac{1}{\sqrt{|l_c|!}} \left(\frac{\sqrt{2}r}{w}\right)^{|l_c|} \times \left(\frac{2r^2}{w^2}\right) e^{-r^2/w^2} e^{il_c\varphi}. \tag{39}$$

With $r = \sqrt{x^2 + y^2}$ and $\phi = tg^{-1}y/x$. In figures 7 and 8, we show the intensity (figure 7) and phase (figure 8) profiles of the generated OAM mode as a function of x and y for different winding numbers $l_c = 0, 1, 2, 3$. In our analysis, we have taken T_e to be equal to 1, w to be 0.5 mm, and Ω_p to be 0.1γ, while keeping all other parameters the same as in figure 2. It is worth noting that for $l_c = 0$, the third generated field's intensity profile demonstrates a Gaussian profile. However, for nonzero l_c values, the doughnut intensity profiles exhibit a dark (blue) hollow center, indicating the conserved transfer of optical vortex of the probe beam to the generated third beam. For larger topological charges lc, the doughnut diameter increases. The helical phase patterns allow for an understanding of the singularity at the core of the generated third OAM beam. When $l_c = 0$, no singularity occurs in the phase patterns, confirming a Gaussian-shaped wavefront of the laser field with a normal phase. For nonzero vorticities, the phase patterns begin to twist.

4. Conclusion

In summary, our study has focused on the electron tunneling effect in an QD molecule exhibiting multi-wave mixing efficiency. It is observed that the new generated laser field is yet to be established at the commencement of the ensemble, wherein the feeble probe beam has just infiltrated. As the beam propagates within the QD ensemble, the new field is produced. Analytical solutions elucidate that the beam created undergoes energy losses, predominantly at the inception of the ensemble. However, as the beam penetrates deeper into the ensemble, the losses subside, and the system transitions into a state of transparency. Furthermore, we have observed that the new generated light can be amplified through the medium by adjusting the relative phase between applied lights and the detuning of the probe light. Moreover, we have discussed the group velocity properties of the generated light by adjusting the relative phase of the applied lights. At the end, we have demonstrated that the inter-dot tunneling phenomenon can bring about the transfer of OAM between various frequencies.

A specific scenario has been taken into account where a strong coupling beam is initially a vortex beam. As a result of the impact of tunneling coupling, an additional laser is produced with the identical winding number as that of the incident coupling field.

References

[1] Wu Y and Yang X 2005 *Phys. Rev.* A **71** 053806
[2] Vafafard A, Sahrai M, Hamedi H R and Asadpour S H 2020 *Sci. Rep.* **10** 1–10
[3] Asadpour S H, Kirova T, Qian J, Hamedi H R, Juzeliūnas G and Paspalakis E 2021 *Sci. Rep.* **11** 1–11
[4] Aichun L, Wenjuan F, Ying B, Lianglong F and Guanzhong L 2022 *Chin. J. Phys.* **77** 2589–602
[5] Solookinejad G, Jabbari M, Nafar M, Ahmadi E and Asadpour S 2018 *J. Appl. Phys.* **124** 063102
[6] Wu Y and Yang X 2007 *Appl. Phys. Lett.* **91** 094104
[7] Wu Y, Saldana J and Zhu Y 2003 *Phys. Rev.* A **67** 013811
[8] Wu Y and Deng L 2004 *Phys. Rev. Lett.* **93** 143904
[9] Wu Y 2005 *Phys. Rev.* A **71** 053820
[10] Ge G Q, Li H C and Zubairy M S 2020 *Phys. Rev.* A **102** 053701
[11] Zheng H, Nie Z, Li P, Yang Y, Zhang Y and Xiao M 2008 *Phys. Rev.* A **77** 063829
[12] Asadpour S H, Faizabadi E, Kudriašov V, Paspalakis E and Hamedi H 2021 *Eur. Phys. J. Plus* **136** 1–13
[13] Asadpour S H, Paspalakis E and Hamedi H R 2021 *Phys. Rev.* A **103** 063705
[14] Asadpour S H, Abbas M and Hamedi H R 2022 *Phys. Rev.* A **105** 033709
[15] Chen H J 2020 *Laser Phys. Lett.* **17** 025201
[16] Naseri T 2020 *Phys. Lett.* A **384** 126164
[17] Delir Ghaleh Joughi Y and Sahrai M 2022 *Sci. Rep.* **12** 7984
[18] Liu Y, Xiang Y and Mohammed A A 2022 *Laser Phys. Lett.* **19** 095205
[19] Wang Z, Qiu J, Ding D, Li W and Yu A B 2018 *Opt. Express* **28** 2975
[20] Sun D, Zhang H, Sun H, Li X and Li H 2018 *Laser Phys. Lett.* **15** 045208
[21] Chen G, Stievater T H, Batteh E T, Li X, Steel D G, Gammon D, Katzer D S, Park D and Sham L J 2002 *Phys. Rev. Lett.* **88** 117901
[22] Villas-Bôas J, Govorov A and Ulloa S E 2004 *Phys. Rev.* B **69** 125342
[23] Yuan C-H and Zhu K-D 2006 *Appl. Phys. Lett.* **89** 052115
[24] Hamedi H R 2014 *Laser Phys. Lett.* **11** 085201
[25] Arzhang B, Mehmannavaz M and Rezaei M 2015 *Laser Phys.* **25** 125202
[26] Tian S C, Wan R-G, Tong C-Z, Fu X-H, Cao J-S and Ning Y Q 2015 *Laser Phys. Lett.* **12** 125203
[27] Wang Z, Zhen S and Yu B 2015 *Laser Phys. Lett.* **12** 046004
[28] Peng Y, Yang A, Chen B, Zhang S, Liu S and Wang X 2016 *Laser Phys. Lett.* **13** 025401
[29] You Y, Qi Y H, Niu Y P and Gong S Q 2019 *J. Phys.: Condens. Matter* **31** 105801
[30] Al-Toki H G and Al-Khursan A H 2020 *Opt. Quantum Electron.* **52** 1–22
[31] Abo-Kahla D 2021 *Indian J. Phys.* **95** 1295–304
[32] Duchet M, Perisanu S, Purcell S T, Constant E, Loriot V, Yanagisawa H, Kling M F, Lepine F and Ayari A 2021 *ACS Photonics* **8** 505–11
[33] Wu Y and Yang X 2004 *Phys. Rev.* A **70** 053818